

# STUDY ON EARTHQUAKE DESTRUCTION MODE OF THE LARGEST CANAL CROSSING HIGHWAY BRIDGE BASED ON IEM BOUNDARY IN SOUTH-TO-NORTH WATER DIVERSION

Xinyong Xu<sup>1,2,3</sup>, Honghao Zhang<sup>1</sup>, Jinchang Liang<sup>1</sup>, Xuhui Liu<sup>1</sup>, Chenlong Xie<sup>4</sup> and Jianwei Zhang<sup>1,2,3</sup>

1. North China University of Water Resources and Electric Power, School of Water Conservancy, Zhengzhou 450046, China; xuxinyong@ncwu.edu.cn
2. Collaborative Innovation Center of Water Resources Efficient Utilization and Protection Engineering, Henan Province, Zhengzhou 450046, China
3. Henan Hydraulic Structure Safety Engineering Technology Research Center, Zhengzhou 450046, China
4. Shanghai Investigation, Design & Research Institute Co., Ltd., Shanghai 200092, China

## ABSTRACT

To study the dynamic failure mechanism and damage development law of highway bridge structure under the boundary effect in the process of seismic dynamic duration, the Wenchang Highway Bridge with the largest canal crossing in the South-to-North Water Diversion is taken as an example for seismic design analysis. Based on the finite element and infinite element coupling theory, the infinite element method boundary is introduced, the concrete damage plasticity is introduced, and the half-space free field model is established to study the energy dispersion phenomenon of waves in the boundary and the absorption effect of the infinite element method boundary on wave energy is verified. Under different peak acceleration intensities, the seismic response analysis of the bridge structure was carried out. The results show that: Under the action of selected artificial waves, the damage location of the bridge mainly concentrated in the junction of the box girder supported by the pier, the bottom of the pier and the junction of the pier and beam. The damage tends to develop downward near the bottom of the box girder. The damage at both ends of the beam extends from both ends to the middle. And the bottom and top of the pier have penetrating damage. These are weak points in seismic design. At a horizontal peak acceleration of 0.6 g, in addition to damage to the pier column, damage also occurred to the bottom of the box girder. Therefore, when the horizontal peak acceleration of the seismic wave is greater than 0.6g, the failure of the bottom of the box girder is paid attention to. Moreover, the IEM boundary has a good control effect on the far-field energy dissipation of the wave, which is simpler and more efficient than the viscous-spring boundary.

## KEYWORDS

Cross channel highway bridge for South-to-North Water Diversion, Infinite element method boundary, FE-IE coupling, Plastic damage constitutive, Earthquake damage evolution

## INTRODUCTION

In China, the South-to-North Water Diversion(SNWD) is a major national infrastructure project for the deployment of water resources. Since its commissioning, it has effectively alleviated the severe water shortage in the Yellow-Huai-Hai plains of northern China. Study [1] has shown that the middle route of the SNWD has significant positive benefits for the sustainable stabilization and restoration of groundwater in northern China. The middle route of the SNWD is 1432 km long and

spans numerous rivers, highways, railroads, valleys, washes and other projects in the whole area. Many bridges crossing the SNWD are in high seismicity regions. To ensure the safety of these bridges after an earthquake, seismic analysis of them is necessary to clarify their seismic failure characteristics.

The Wenchang Highway Bridge is the largest cross-canal highway bridge in the middle route of the SWND. Its structure is a high-pier and large-span cast-in-place concrete box girder bridge. Its site is located in a 7-degree fortification intensity area. As a bridge spanning major national livelihood projects, its seismic performance is not only related to the safety of water quality, but also to the impact of structural safety. Therefore, it's particularly significant to study the dynamic failure mechanism and damage development law of the bridges crossing the SNWD.

There have been many research results on bridge seismic problems. Based on the damage index, Xie and Sun [2] analyzed the seismic damage and failure mode of the cable-stayed bridge. They concluded that the seismic frequency has a significant impact on structural damage. Deng et al. [3] found that the chain collision effect between the main bridge and multiple approach bridges at the expansion joints will affect the seismic performance of the whole bridge. Zhu and Jiang [4] comprehensively considered the energy and deformation requirements, discussed the seismic method of bridge single pier based on damage performance. Tongaonkar et al. [5] suggested that the interaction between piles and soil will significantly affect the displacement response of the isolated bearing. Shi et al. [6] analyzed the seismic damage mode of the high pier and long-span bridge during the typical construction stage. Combined with the failure limit of each component, Guo et al. [7] analyzed the failure mode of multi-span simply supported beams under earthquake action. Wang et al. [8] analyzed the dynamic response and failure law of the bridge under the combined action of earthquake and blasting. Farahmand-Tabar et al. [9] evaluated the performance of cable-stayed arch Bridges under orthotropic three-component earthquakes. Li et al. [10] studied the effect of soil spatial variability on the seismic performance of SCCS bridges. Li and Xu [11] proposed a hybrid seismic control system combining three-dimensional hybrid seismic isolation bearings and longitudinal fluid viscous dampers. Chu et al. [12] used the modified Morison equation to calculate the hydrodynamic pressure, and analyzed the influence of the water immersion depth on the dynamic response of the arch bridge. Deng et al. [13] took a typical multi-span continuous girder bridge with a pedestal abutment as the research object to analyze the longitudinal seismic performance of the bridge under different abutment stress conditions. Addressi et al. [14] evaluated and monitored the nonlinear dynamic response of the structure from the aspects of top shift time course, global damage index evolution and damage variable distribution.

Throughout the above research, the law of seismic damage of bridge structure is mainly considered, and the influence of infinite foundation on seismic calculation is not fully considered. The energy propagation of seismic wave and the reflection effect of wave on the boundary has an important impact on obtaining reasonable results for the dynamic calculation.

When solving structural dynamics problems, the infinite domain foundation simulation is the key of calculation and analysis. Lysmer and Kuhlemeyer [15] proposed the earliest simple viscous boundary, but it is not suitable for the multi-dimensional wave problems of complex structures. Deek et al. [16] studied the soil-structure interaction effect, striving to solve the transient SSI effect. Liu et al. [17] derived viscoelastic boundary equation based on wave equation and verified accuracy and stability of the three-dimensional viscoelastic artificial boundary. He et al. [18] simplified the implementation method of viscoelastic boundary, which greatly improved the calculation efficiency. Liao et al. [19] proposed and improved the transmission boundary formula, which moderately improves the accuracy, but the implementation process is complex. The infinite element method (IEM) boundary is a method proposed to overcome the problem of infinite domain solved by finite element method. It has inherent coordination with finite element method, and has some advantages than other numerical methods for solving infinite domain problems. Ungless [20] first proposed the concept of the infinite element in 1973. In 1982, Chow et al. [21] proposed the resonant infinite solid element and introduced the infinite element study into the propagation analysis of waves in solids. Bettess [22] put forward the concept of mapping infinite element for the

first time. Asheghabadi et al. [23] compared the calculation results under two boundary conditions of the IEM boundary and viscous boundary and found that the IEM boundary can be realized in less calculation time. Qi et al. [24] verified the applicability of the IEM boundary. Compared with viscoelastic boundary, the IEM boundary can better filter the scattered waves. Zhang et al. [25] applied this method to foundation structure dynamic interaction analysis earlier. As a method to solve three-dimensional multi-directional mapping problems, the IEM boundary has not been widely used in engineering.

Based on the commercial software ABAQUS, modeling and analysis are carried out. In this paper, the IEM boundary is used for seismic wave input. In order to explore the dynamic failure mechanism and damage development law of the concrete highway bridge under ground motion, the concrete damage plasticity (CDP) theory is introduced. This study hopes to provide references and a scientific basis for the large cross canal highway bridges' seismic design.

### INFINITE ELEMENT METHOD BOUNDARY

The IEM boundary absorbs the seismic wave energy by introducing a built-in damper on the model boundary to weaken the reflection and scattering effect of the seismic wave at the boundary.

Considering that the medium is endowed with linear elastic properties, its equilibrium equation is

$$-\rho\ddot{u} + \frac{\partial}{\partial x} \cdot \sigma = 0 \quad (1)$$

where  $\rho$  is the density, kg/m<sup>3</sup>;  $\ddot{u}$  is the acceleration, m/s<sup>2</sup>;  $\sigma$  is stress, Pa;  $x$  is the location. Assuming that the material is isotropic and linear elastic, the stress  $\sigma$  can be expressed as

$$\sigma = \lambda \mathbb{I} : \varepsilon + 2G\varepsilon \quad (2)$$

where  $\varepsilon$  is the strain;  $\lambda$  is lame constant,  $\lambda = \frac{E\nu}{(1+\nu)(1-2\nu)}$ ;  $G$  is shear modulus,  $G = \frac{E}{2(1+\nu)}$  ( $E$  is Young's modulus,  $\nu$  is Poisson's ratio);  $\varepsilon$  is assumed to be a small strain.

$$\varepsilon = \frac{1}{2} \left\{ \frac{\partial u}{\partial x} + \left[ \frac{\partial u}{\partial x} \right]^T \right\} \quad (3)$$

The governing equation of motion is expressed as

$$\rho\ddot{u}_i = G \frac{\partial^2 u_i}{\partial x_j \partial x_j} + (\lambda + G) \frac{\partial^2 u_j}{\partial x_i \partial x_j} \quad (4)$$

Assuming that the plane wave moves along the X-axis, equation (5) expresses the longitudinal wave, and equations (6) and (7) express the shear wave.

$$u_x = f(x \pm c_p t), u_y = u_z = 0 \quad (5)$$

$$u_y = f(x \pm c_s t), u_x = u_z = 0 \quad (6)$$

$$u_z = f(x \pm c_s t), u_x = u_y = 0 \quad (7)$$

where  $c_p = \sqrt{\frac{\lambda+2G}{\rho}}$ ,  $c_s = \sqrt{\frac{G}{\rho}}$ , "-" indicates forward propagation along X, "+" indicates backward propagation along X.

The infinite element absorbs the radiation energy of plane body wave by introducing damping coefficient  $d_p$  and  $d_s$  on the boundary. It is assumed that the infinite element material is linear elastic, and the stress generated by damping is shown in formula (8) ~ (10)

$$\sigma_{xx} = ma - d_p \dot{u}_x \quad (8)$$

$$\sigma_{xy} = -d_s \dot{u}_y \quad (9)$$

$$\sigma_{xz} = -d_s \dot{u}_z \quad (10)$$

where for longitudinal waves, the stress at the boundary ( $x = L$ ) is  $\sigma_{xx} = (\lambda + 2G)(f_1' + f_2')$ . The rest of the stress components are  $\sigma_{ij} = 0$ . The speed is  $\dot{u}_x = -c_p(f_1' - f_2')$ , and can be concluded from the above formula

$$(\lambda + 2G - d_p c_p) f_1' + (\lambda + 2G + d_p c_p) f_2' = 0 \quad (11)$$

When  $f_2 = 0$  and  $f_2' = 0$ , we can ensure that no reflection stress wave is generated at the boundary under any incident condition. Therefore, the longitudinal wave and the shear wave damping form can be calculated by the following formula.

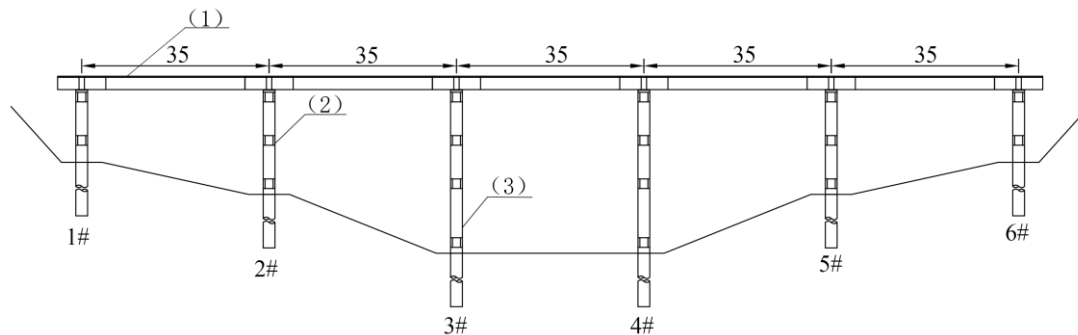
$$d_p = \frac{\lambda + 2G}{c_p} = \rho c_p \quad (12)$$

$$d_s = \rho c_s \quad (13)$$

IEM achieves FEM-IEM coupling by processing boundary. The IEM boundary is equivalent to the absorption boundary. In order to ensure that the seismic wave has no reflection under any incident condition, the damping coefficients are introduced into the element itself.

## PROJECT OVERVIEW

In this study, the Wenchang Highway Bridge, the largest cross canal highway bridge in the middle route of SNWD, is selected as a case, as shown in Figure 1.



(1) Box girder; (2) Cross beam; (3) Pier

Fig. 1 - General Arrangement of Wenchang Highway Bridge (Unit: m)

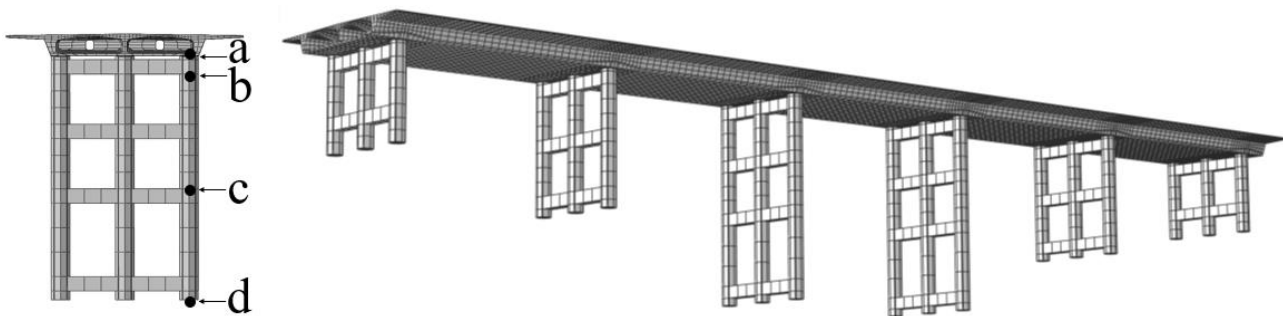
The total length of the box girder bridge is 175m with 5 spans. The double box girder's width is 28 m and the height is 2.71m. The model material parameters are shown in Table 1.

Tab. 1 - The Bridge's Material Parameters

Material	Box girder (C50)	Pier (C30)	Foundation soil layer	Foundation rock layer
Young's modulus (GPa)	34.5	30	0.04	10
Density (kg/m <sup>3</sup> )	2430	2400	1796	2100
Poisson ratio	0.2	0.2	0.3	0.3
Tensile strength (Mpa)	1.83	1.39	-	-
Compressive strength (Mpa)	24.4	13.8	-	36.1

## FINITE ELEMENT MODEL

Figure 2 depicts the whole 3D bridge numerical simulation structure model, and the FEM-IEM coupling foundation model is established (Figure 3), where the seismic wave acceleration is applied at the bottom of a compartment at the FE-IE coupling. The definition of the overall coordinates is as follows: take the center of the box girder bottom as the coordinate origin. The x-axis is the channel flow direction, and the downstream direction is positive; the y-axis is the vertical direction, and the upward direction is positive; the z-axis is the longitudinal axis direction of the bridge deck, and the north direction is positive.



Local 3#

Overall structure of the bridge

Fig. 2 - Three-Dimensional Finite Element Calculation Model

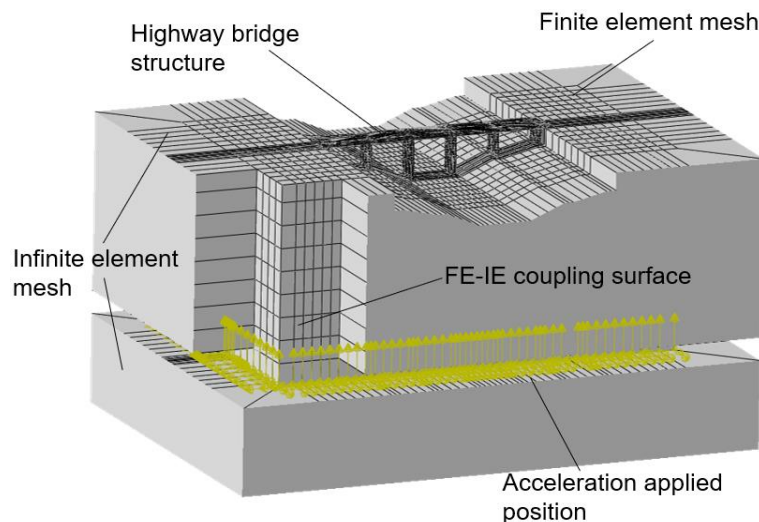
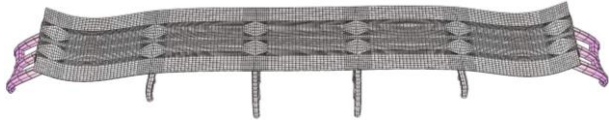

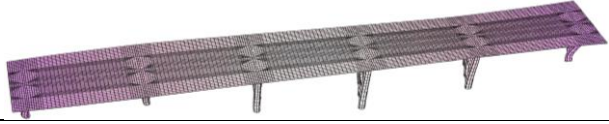
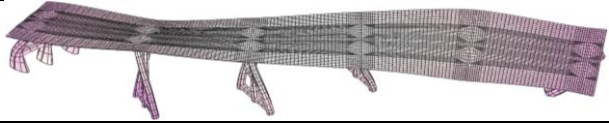


Fig. 3 - FEM-IEM Coupling Foundation Model

## MODAL ANALYSIS OF BRIDGE STRUCTURE

Table 2 shows the first four vibration modes of the bridge structure. In this paper, Rayleigh damping is used for the analysis, and take the damping ratio corresponding to the frequency of the structure as 5%, and determine the damping constants according to the first two natural frequencies of the structure as 0.681Hz and 0.697Hz, and the damping constants  $\alpha = 0.216$  and  $\beta = 0.011$ .

Tab. 2 – The first four frequencies and vibration modes of the bridge structure

Mode Number	Modal	Vibration Modes
1		Transverse
	0.681Hz	
2		Transverse
	0.697Hz	
3		Transverse
	0.700Hz	
4		Vertical
	0.714Hz	

## SELECTION OF SEISMIC WAVE

According to the site type and seismic area division of the bridge, the seismic fortification intensity of this site is VII and the site type is class I. The horizontal peak acceleration of the corresponding rare earthquake is 0.2g, and the vertical peak acceleration is 2/3 of the horizontal direction.

Since there are few natural seismic waves recorded at the location of the bridge, the seismic wave input that occurred in the past cannot truly simulate the failure of the bridge, and the artificial wave can well match the characteristics of the target response spectrum, so the artificial wave is fitted according to the basic data of the project and the characteristics of the seismic wave. The RH1TG040 artificial seismic wave is chosen for computation based on the spectral proximity principle. Its peak acceleration is 0.2g. The acceleration time history curve in the main direction is shown in Figure 4, and the ground motion input interval is 0.02 s. This calculation's total duration is 30 s. The acceleration response spectrum is shown in Figure 5, where the black line represents the target response spectrum and the red line represents the RH1TG040 response spectrum. In order to show the failure law of the bridge structure, the horizontal peak acceleration of artificial seismic waves was adjusted to 0.2g, 0.4g, 0.6g, 0.8g and 1.0g, and the seismic response analysis of the structure at different intensities was carried out.

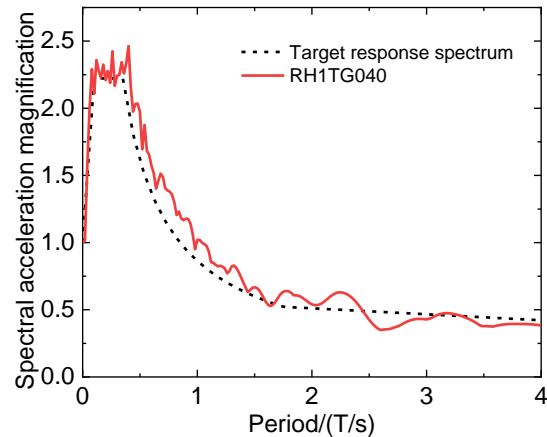
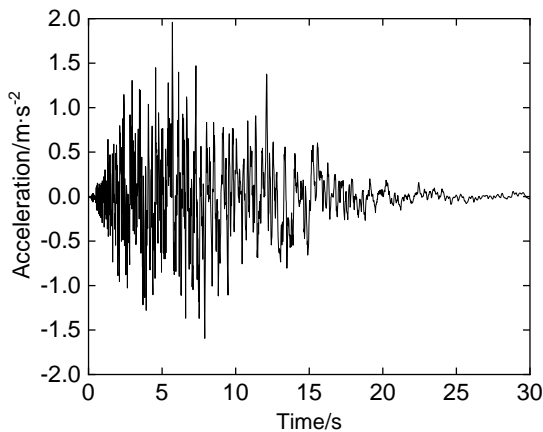


Fig. 4 - Ground Acceleration Time History Curve Fig. 5 - Acceleration response spectrum curves

## SEISMIC RESPONSE LAW AND DAMAGE MECHANISM OF THE BRIDGE

### Acceleration response law of bridge structure

Select 3# bridge box girder bottom plate point a, pier top point b, pier mid-point c and pier bottom point d as the representative characteristic points respectively for bridge seismic dynamic response analysis, and artificial waves with a peak acceleration of 0.2g in the horizontal ground motion are selected for analysis, and the characteristic points are shown in Figure 2.

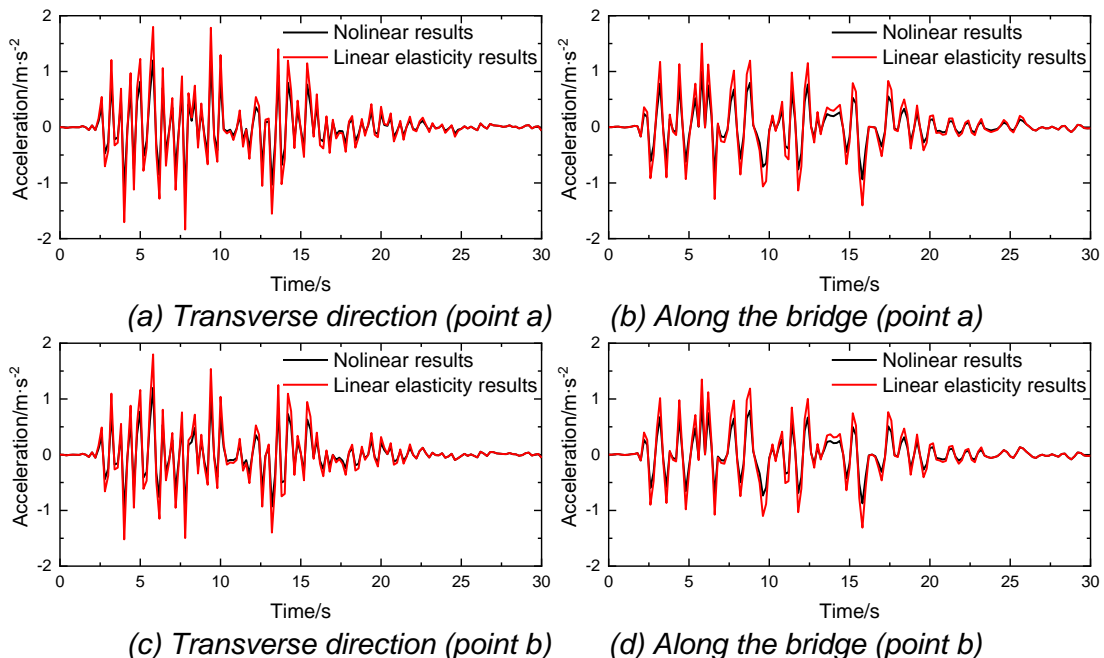


Fig. 6 - Comparison Diagram of Acceleration Time History of Characteristic Points

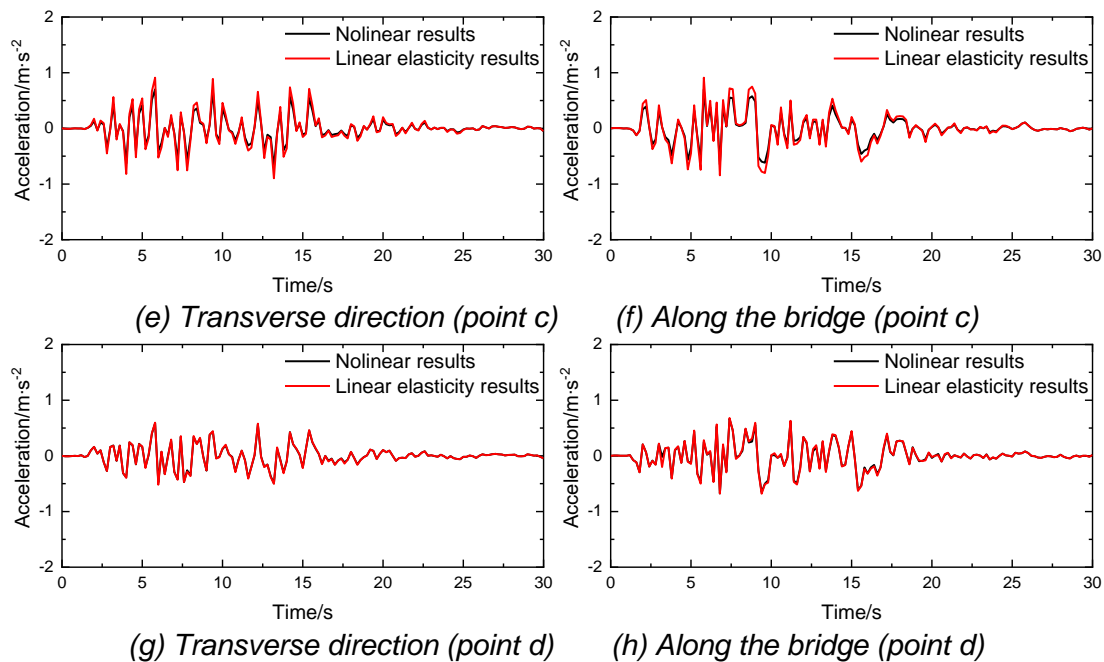


Fig. 6 - Comparison Diagram of Acceleration Time History of Characteristic Points

Through the acceleration time history of the bridge structure in Figure 6, we can get the following conclusions. (1) The acceleration development trend of each characteristic point under the IEM boundary is basically the same, and the maximum response appears in the earthquake lasting about 6 s. This is about the same time as the earthquake's peak acceleration. (2) In the process of the strong earthquake, considering the plastic damage and the law of velocity change, compared with the results without considering the damage, the accumulation of plastic damage occurs in the material, and the real-time change of concrete elastic modulus leads to more frequent fluctuation changes. (3) The higher the height of the structure where the feature point is located, the greater the acceleration. The lower position's response of the pier is less than the higher position's and the middle of the box girder.

### Displacement response law of bridge structure

The above comparison of the acceleration time history curve results considering nonlinear and linear elasticity shows the rationality of considering plastic damage, and considering plastic damage in engineering practice can more realistically reflect the ground motion response characteristics of bridges. Figure 7 depicts the displacement variation law of each characteristic point of the bridge under different horizontal peak acceleration considering plastic damage. Through this figure, we can see that: (1) Under earthquake action, when the time reaches about 6 s, the displacement of each characteristic point reaches the peak the first time. Seismic peak acceleration also appears at this time, and the occurrence time of these two peak times is the same. (2) The horizontal displacement along the bridge of each part is greater than the horizontal displacement across the bridge, which indicates that the stiffness of the structure across the bridge is greater, so we should pay attention to the change law of the displacement along the bridge. (3) With the gradual increase of peak acceleration, the displacement of each feature point is also large, because the structure has a large plastic deformation, indicating that the peak acceleration of seismic waves has a significant impact on the displacement of the bridge structure. (4) In the early stage of earthquake action, the bridge structure is still in the elastic state due to the small seismic excitation. Whether to consider the damage on the structural displacement response is not significant. In the later stage of the earthquake, as the peak acceleration of ground motion



gradually increases, the displacement response of the feature points to the structure has a certain displacement deviation relative to the foundation and gradually increases, mainly because the softening behavior of the concrete structure after damage can be described after the introduction of the CDP constitutive model. Irreversible plastic damage occurred in the structure during the earthquake.

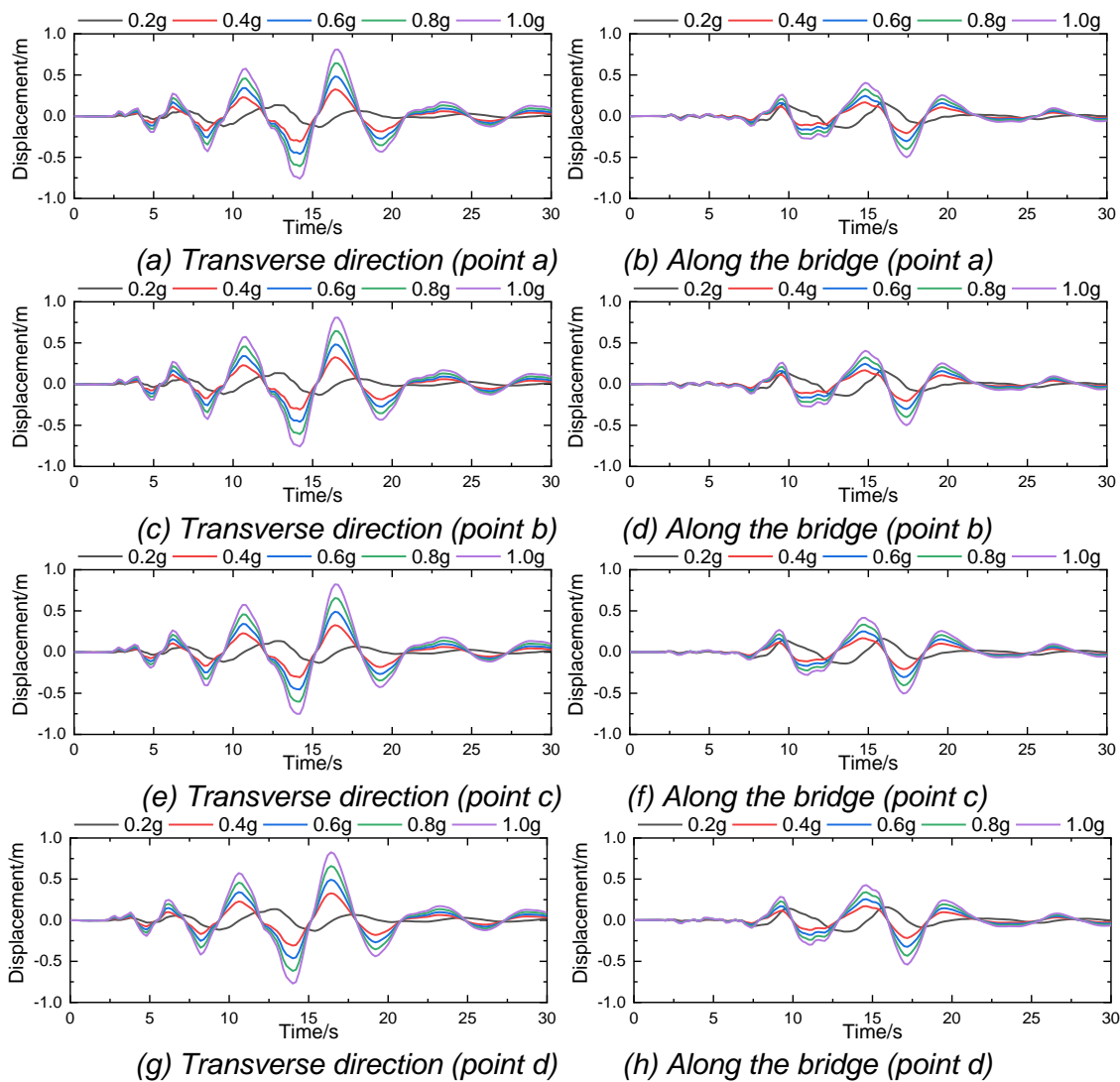


Fig. 7 - Comparison of the Displacement Time History of Each Feature Point

### Dynamic damage mechanism of bridge structure

Figure 8, Figure 9 and Figure 10 describe the development process of bridge structure damage when the horizontal peak acceleration is 0.2 g, 0.4 g, and 0.6 g, respectively. Under the action of 0.2g and 0.4g horizontal peak acceleration, the damage was mainly distributed at the junction between the bottom of the box girder and the pier, the junction between the beam end and the pier, and the bottom of the pier. As the horizontal peak acceleration of the input gradually increases, the damage range of the pier column also gradually increases. At a horizontal peak acceleration of 0.6 g, in addition to damage to the pier column, damage also occurred to the bottom of the box girder.

From the perspective of damage development process, at 2.4 s, the bottom of the pier column appeared for the first time under the artificial wave of these three ground motion strengths, and then at 3.2 s, the damage appeared near the box girder near the pier support, as shown in the Figures 8 (a) ~ (b), 9 (a) ~ (b), 10 (a) ~ (b). In the duration of 3.2 s ~ 6.0 s, the damage range gradually extends from the top and bottom piers to the middle, as shown in the figure. 8 (b) ~ (c), 9 (b) ~ (c), 10 (b) ~ (c). During 6.0 s~11.2 s, the damage expands from the bottom of the box girder and the bottom of the pier to the middle of the pier, as shown in the figure. 8 (d), 9 (d), 10 (d). In the later stages of the earthquake, the loss is basically unchanged due to the decrease in the acceleration of the earthquake.

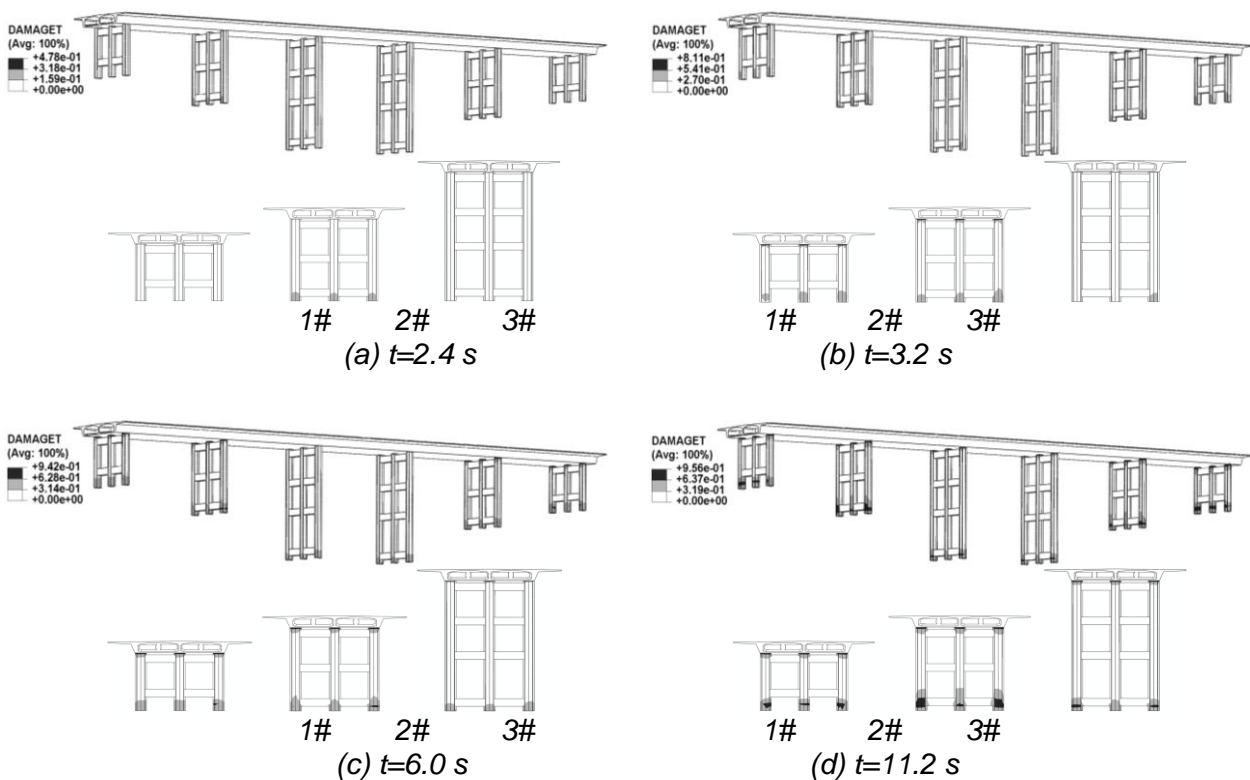


Fig. 8 - Developing Process of Bridge's Damage Under Earthquake(0.2g)

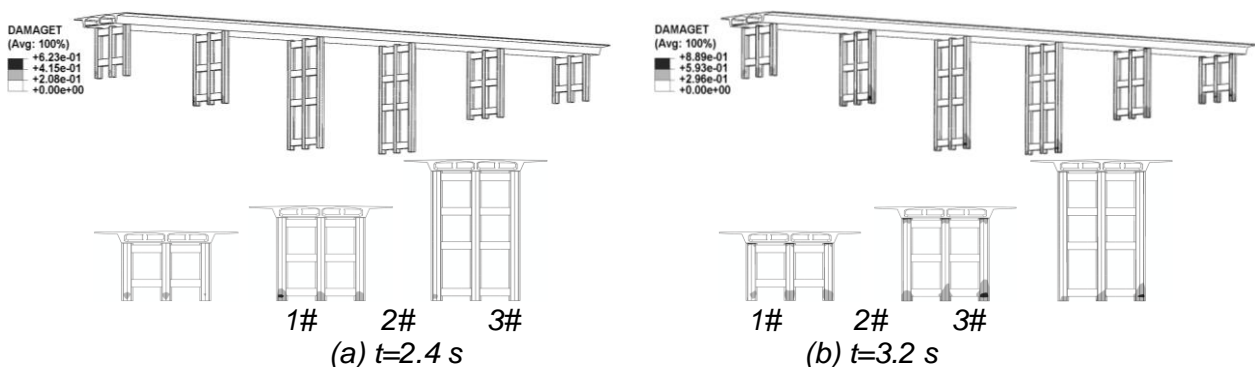


Fig. 9 - Developing Process of Bridge's Damage Under Earthquake(0.4g)

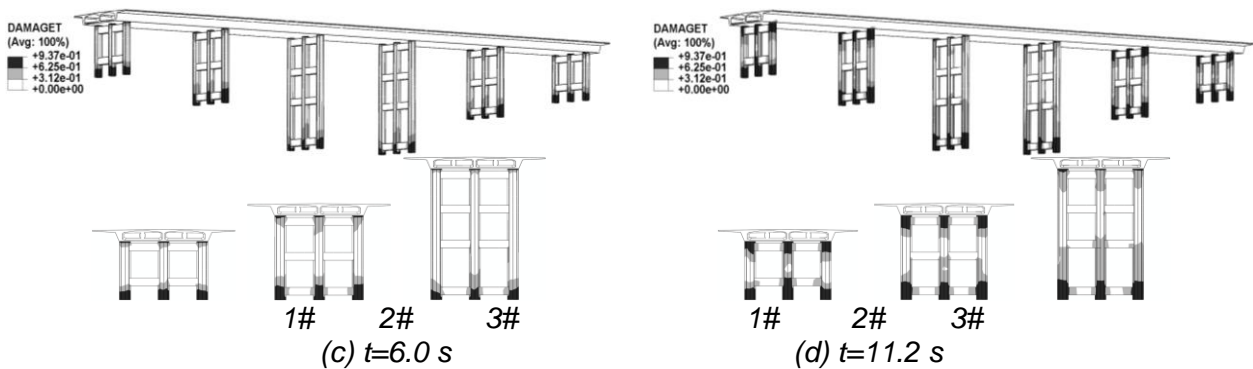


Fig. 9 - Developing Process of Bridge's Damage Under Earthquake(0.4g)

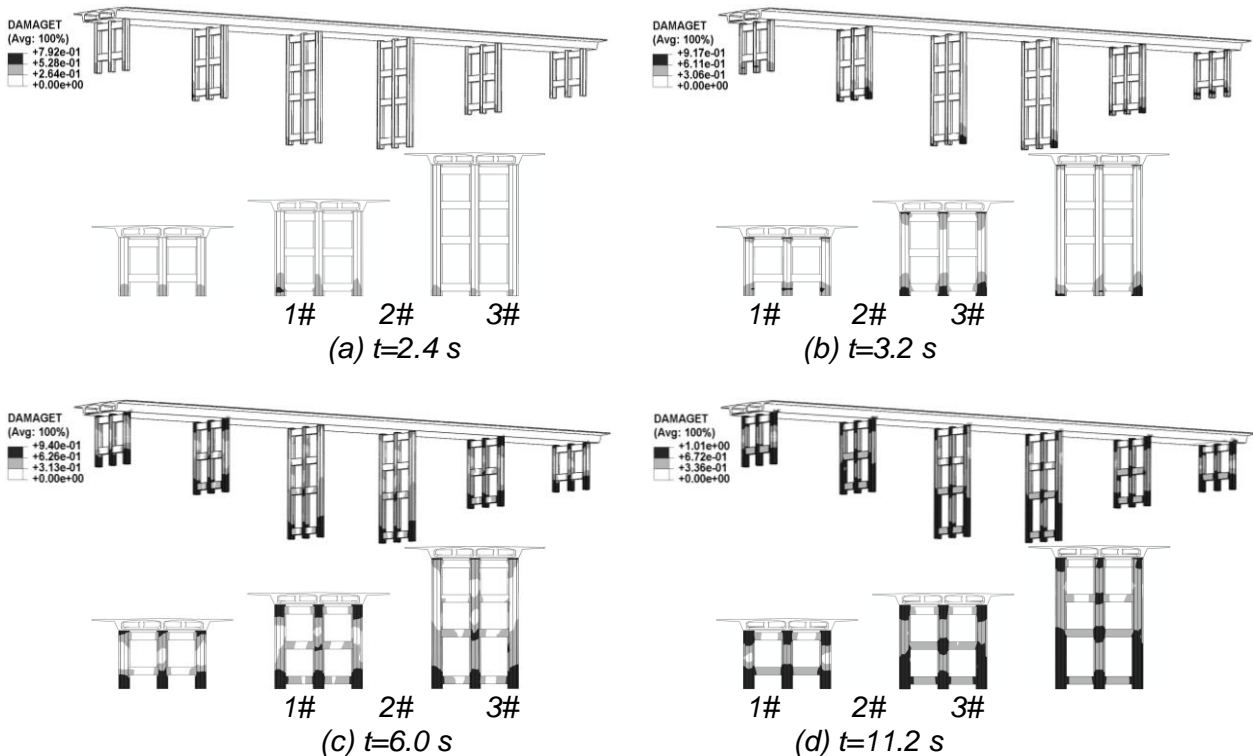


Fig. 10 - Developing Process of Bridge's Damage Under Earthquake (0.6g)

In order to further study, the damage process and development law of the bridge under the action of earthquake, the damage development process analysis of the feature points under different horizontal peak accelerations is carried out, and Figure 11 describes the development and change of the damage values of each feature point. Through this figure, we can see that: (1) The bottom of the pier column where the feature point D is located is the first to be damaged, and with the continuous action of seismic force, after the damage occurs at the bottom of the pier column, the damage range rapidly extends to the entire pier column. (2) Compared with the damage development time of each feature point, the damage rate of the bottom of the box girder where feature point A is located is obviously backward and the damage range is small, and the damage development rate at the bottom of the pier column where feature point D is located is the fastest and the damage value is large. (3) When the horizontal peak acceleration is 0.2g, only the feature

point d has obvious damage. (4) With the gradual increase of peak acceleration, the greater the damage of each feature point, and the damage peak of each feature point is reached in the range of 11 s~18 s, and the damage tends to be stable after 18 s. The bridge damage obtained above was obtained only for the manual records selected in the study.

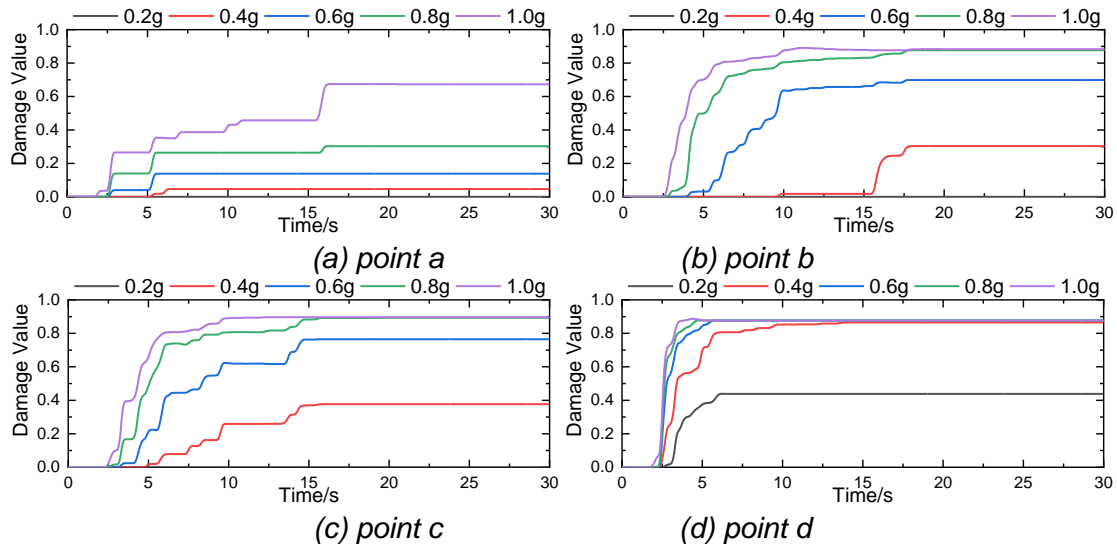


Fig. 11 - Feature point damage development process

## CONCLUSION

In this study, the Wenchang Highway Bridge is taken as the actual engineering background to carry out the seismic response analysis. In the meantime, the seismic performance of the cross canal highway bridge is evaluated according to the design requirements. We get some conclusions as follows:

- (1) The IEM boundary can well absorb the incident wave's energy and the results are accurate and reasonable. Compared with the viscous-spring boundary, the IEM boundary doesn't need to set a spring-damper system. At the same time, it can also simulate the case of zero displacement at infinity, which can make up for the lack of calculation due to the limitation of boundary conditions. It provides a new reference for the treatment of the boundary in the dynamic calculation of bridge structure.
- (2) In the acceleration response analysis of bridge structures, the acceleration response increases with the increase of the height of the structure. The fluctuation of the nonlinear acceleration response curve of the characteristic points of the bridge structure was more obvious, and the nonlinear and linear elastic acceleration response results of the characteristic points of the bridge structure differ by 0.1% ~ 33.3%.
- (3) Under the action of selected artificial waves, the damage location of the bridge mainly occurs in the following three parts: the connection of the box girder near the pier support, the bottom of the pier, and the connection between the pier column and the beam, which is the weak link of the bridge structure.
- (4) In the analysis of the damage development process, under the action of the horizontal peak acceleration of 0.6g, in addition to the damage of the pier column, the bottom of the box girder also appeared damage. Therefore, when the horizontal peak acceleration of the seismic wave is greater than 0.6g, the failure of the bottom of the box girder is paid attention to.

## ACKNOWLEDGEMENTS

This study was supported by the National Key Research and Development Program of China (Grant No. 2018YFC0406901), the National Natural Science Foundation of China (Grant No. 51979109) and Henan Province University Science and Technology Innovation Team Support Plan (Grant No. 19IRTSTHN030). These supports are gratefully acknowledged and greatly appreciated.

## REFERENCES

- [1] Long D., Yang W., Scanlon B.R., et al., 2020. South-to-North Water Diversion stabilizing Beijing's groundwater levels. *Nature Communications*, vol. 11: 1-10. <http://doi.org/10.1038/s41467-020-17428-6>
- [2] Xie W., Sun L. M., 2014. Study on Seismic Damage and Failure Patterns of Super Long-Span Cable-Stayed Bridge under Earthquake. *Earthquake Engineering & Engineering Dynamics*, vol.1 : 127-135. <http://doi.org/10.13197/j.eeev.2014.06.127.xiew.017>
- [3] Deng Y. L., Lei F., He X. J., 2015. Study on Effects of Pounding at Expansion Joints on Seismic Responses of Long-Span Cable-Stayed Bridges between Main Span and Multiple Approach Spans under Earthquakes. *China Civil Engineering Journal*, vol. 48: 87-95. <http://doi.org/10.15951/j.tmgcxb.2015.02.013>
- [4] Zhu X., Jiang H., 2009. Performance-Based Seismic Design Method for Rc Bridge Piers. *China Civil Engineering Journal*, vol. 42 : 85-92.
- [5] TONGAONKAR N. P., JANGID R. S., 2003. Seismic response of isolated bridges with soil–structure interaction. *Soil Dynamics and Earthquake Engineering*, vol. 23: 287-302. [http://doi.org/10.1016/S0267-7261\(03\)00020-4](http://doi.org/10.1016/S0267-7261(03)00020-4)
- [6] Shi Y., Zhang F. J., Han J. P., et al., 2020. Seismic damage analysis of a long-span continuous rigid frame bridge with high piers during typical construction stages. *Zhendong yu Chongji/Journal of Vibration and Shock*, vol. 39 : 89 - 95. <http://doi.org/10.13465/j.cnki.jvs.2020.22.013>
- [7] Guo W., Wang Y., Ge C. Y., et al., 2020. Seismic failure features of multi-span simply supported girder bridges of high-speed railway under near-fault earthquake. *Zhendong yu Chongji/Journal of Vibration and Shock*, vol. 39 : 210-218. <http://doi.org/10.13465/j.cnki.jvs.2020.17.028>
- [8] Wang J. Y., Yuan W. C., 2020. Numerical simulation of the response and damage of girder bridges subjected to the combined action of earthquake and blast. *Harbin Gongcheng Daxue Xuebao/Journal of Harbin Engineering University*, vol. 41 : 643-649. <http://doi.org/10.11990/jheu.201812013>
- [9] Farahmand-Tabar S., Barghian M., 2020. Seismic assessment of a cable-stayed arch bridge under three-component orthotropic earthquake excitation. *Advances in Structural Engineering*, vol. 24 : 227–242. <http://doi.org/10.1177/1369433220948756>
- [10] Li C., Diao Y., Li H.-N. et al., 2023. Seismic performance assessment of a sea-crossing cable-stayed bridge system considering soil spatial variability. *Reliability Engineering & System Safety*, vol. 235: 109210. <http://doi.org/10.1016/J.RESS.2023.109210>
- [11] Li J., Xu L., 2023. Seismic performance improvement of continuous rigid-frame bridges with hybrid control system under near-fault ground motions. *Soil Dynamics and Earthquake Engineering*, vol. 168: 107858. <http://doi.org/10.1016/J.SOILDYN.2023.107858>
- [12] Chu Y., Li R., Li X., 2022. Analysis of Seismic Response of the Arch Bridge across Reservoir considering Fluid-Solid Coupling Effect. *Shock and Vibration*, vol. 2022. <http://doi.org/10.1155/2022/3873935>
- [13] Deng Y., Ge S., Lei F., 2023. Effects of Pounding and Abutment Behavior on Seismic Response of Multi-Span Bridge Considering Abutment-Soil-Foundation-Structure Interactions. *Buildings*, vol. 13: 260. <http://doi.org/10.3390/BUILDINGS13010260>
- [14] Addessi D., Gatta C., Nocera M. et al., 2021. Nonlinear dynamic analysis of a masonry arch bridge accounting for damage evolution. *Geosciences*, vol. 11: 343. <http://doi.org/10.3390/GEOSCIENCES11080343>
- [15] LYSMER J., KUHLEMEYER R. L., 1969. Finite dynamic model for infinite media. *Journal of the Engineering Mechanics Division*, vol. 95 : 859-878. <http://doi.org/10.1061/JMCEA3.0001144>
- [16] DEEKS A. J., RANDOLPH M. F., 1994. Axisymmetric time-domain transmitting boundaries. *Journal of Engineering Mechanics*, vol. 120 : 25-42. [http://doi.org/10.1061/\(ASCE\)0733-9399\(1994\)120:1\(25\)](http://doi.org/10.1061/(ASCE)0733-9399(1994)120:1(25))
- [17] Liu J. B., Lv Y. D., 1998. A Direct Method for Analysis of Dynamic Soil-Structure Interaction Based on Interface Idea. *China Civil Engineering Journal*, 1998. vol.83 : 3-5.

- [18] He J. T., Ma H. F., Zhang B. Y., et al., 2010. Method and realization of seismic motion input of viscous-spring boundary. *Journal of Hydraulic Engineering*, vol.41 : 960-969.
- [19] Liao Z. P., Huang K. L., Yang B. P., et al., 1984. A Transmitting Boundary for Transient Wave Analyses. *Science in China Series A-Mathematics, Physics, Astronomy & Technological Science*, vol. 27 : 1063-1076.
- [20] UNGLESS R. F., 1973. Infinite finite element ( University of British Columbia ).
- [21] Chow Y. K., Smith I. M., 1981. Static and periodic infinite solid elements. *International Journal for Numerical Methods in Engineering*, vol. 17 : 503-526. <http://doi.org/10.1002/nme.1620170403>
- [22] BETTESS P., 1984. A new mapped infinite element for exterior wave problems. *Numerical methods in coupled systems*.
- [23] Asheghabadi M. S., Ali Z., 2020. Infinite element boundary conditions for dynamic models under seismic loading. *Indian Journal of Physics*, vol. 94 : 907-917. <http://doi.org/10.1007/s12648-019-01533-4>
- [24] Qi Y. L., Hisanori O., 2014. Study of Abaqus Dynamic Infinite Element Artificial Boundary. *Rock and Soil Mechanics*, vol. 35 : 3007-3012. <https://doi.org/10.16285/j.rsm.2014.10.037>
- [25] Zhang C. H., Zhao C. B., 1987. Coupling method of finite and infinite elements for strip foundation wave problems. *Earthquake engineering & structural dynamics*, vol.15 : 839-851. <https://doi.org/10.1002/eqe.4290150705>